Hyungjoo Yoon[1]
Senior Researcher
Satellite Control System Department,
Korea Aerospace Research Institute,
Daejeon 305-333, Korea
e-mail: drake.yoon@gmail.com

Brett E. Bateman[2]
Postgraduate Student
Department of Physics,
U.S. Naval Postgraduate School,
Monterey, CA 93943
e-mail: batemans2001@att.net

Brij N. Agrawal
Distinguished Professor of Department of
Mechanical and Astronautical Engineering,
Director of Space Research and Design Center,
U.S. Naval Postgraduate School,
Monterey, CA 93943
e-mail: agrawal@nps.edu

Laser Beam Jitter Control Using Recursive-Least-Squares Adaptive Filters

The primary focus of this research is to develop and implement control schemes for combined broadband and narrowband disturbances to optical beams. The laser beam jitter control testbed developed at the Naval Postgraduate School is used for development of advanced jitter control techniques. First, we propose a least quadratic Gaussian feedback controller with integrator for cases when only the error signal (the difference between the desired and the actual beam positions) is available. An anti-notch filter is also utilized to attenuate a vibrational disturbance with a known frequency. Next, we develop feedforward adaptive filter methods for cases when a reference signal, which is highly correlated with the jitter disturbance, is available. A filtered-X recursive least-squares algorithm with an integrated bias estimator is proposed to deal with a constant bias disturbance. Finally, experimental results are provided to validate and compare the performance of the developed control techniques. The designed adaptive filter has a simple structure but shows good jitter rejection performance, thanks to the use of a reference signal. [DOI: 10.1115/1.4003372]

1 Introduction

Optical beam pointing and jitter control has become an important research topic in recent years due to its growing applications such as free-space laser communications, airborne/spaceborne laser weapon systems, adaptive optics, etc. The objective of this research is to aim a laser beam at a target location with minimal beam motion, or jitter, in the presence of disturbance. Narrowband jitter is generally created by mechanical vibrations, for example, rotating/repetitive devices (such as electric motors, combustion engines, and flywheel actuators) and motion of flexible structures (such as solar arrays). Broadband jitter can be caused by atmospheric turbulence, which distributes its energy across a wider frequency band.

In order to achieve efficient jitter control, several control techniques have been proposed in literature (see Ref. [1] and references therein). These techniques can be categorized into two types: *feedback control*, where the controller tries to reduce the jitter only using the error signal (the difference between the desired and actual beam positions) at the target, and *feedforward control*, where the controller can use a reference signal,[3] which is highly correlated with the disturbance source. The most common method in the feedback-type control is the linear-time-invariant (LTI) controller, which includes techniques such as classical proportional-integral-derivative (PID) controller, linear-quadratic-Gaussian (LQG) controller [1,2], and the notch filter [3]. The LTI controllers have been widely used in many practical applications, and thus their performance and characteristics are well studied and understood. However, they generally have fixed structures and parameters and cannot handle time-varying disturbances effectively. In order to optimize the control performance against time-varying disturbances, an adaptive control method is needed. Gibson, Tsao, and their research team published a series of research papers [4–6] on beam jitter control using an adaptive loop based on a multichannel recursive least-squares (RLS) lattice filter algorithm, which was originally developed in Ref. [7]. Their methods show good jitter rejection performance and have an advantage of order-recursiveness. However, they have the structure of a lattice filter, which is more sophisticated than the transversal filter and thus difficult to apply without thorough understanding of it. McEver et al. [8] also proposed adaptive feedback control using the Q-parameterization method.

When a reference signal is available, jitter control performance can be improved using adaptive feedforward control methods. The reference signal is fed into an adaptive filter whose filter gains, or weights, are updated by proper algorithms. While the LTI feedback controller uses the error signal to generate control command, the feedforward adaptive filter uses the error signal at the target to adaptively update the filter parameters to optimize control performance. Watkins and Agrawal [1] and Watkins [9] proposed a filtered-X least-mean-square (FXLMS) adaptive filter method for beam jitter control. The least-mean-square (LMS) adaptive filter is simple yet robust and thus the most common adaptive filter in practice [10,11]. The FXLMS is a LMS filter modified to take the secondary-path dynamics (i.e., the actuator dynamics) into account.

In the present paper, we develop a filtered-X recursive-least-squares (FXRLS) adaptive filter technique. The recursive-least-squares (RLS) algorithm is known to be faster and more accurate than the LMS filter [10,11]. The RLS algorithm is computationally more expensive than the LMS algorithm, but the development of digital computers makes it feasible in practical applications.

The RLS algorithm is modified in two ways. First, it is modified to FXRLS where its reference signal is filtered through a copy of an estimated model of the secondary-path dynamics as done in the FXLMS algorithm. Second, an adaptive bias estimator (BE) is integrated into the FXRLS filter. In order to cancel the dc component of the jitter, a separate compensator [4–6] or an adaptive bias filter (ABF) [1] was used in the literature; however, the proposed algorithm does not need an additional control loop.

An experimental laser jitter control testbed, equipped with fast steering mirrors to correct the beam, has been developed to test various control techniques on vibrational induced jitter. Using this testbed, we experimentally validate the developed beam jitter control algorithms.

[1]Corresponding author.
[2]Present address: U.S. Navy.

Contributed by the Dynamic Systems Division of ASME for publication in the JOURNAL OF DYNAMIC SYSTEMS, MEASUREMENT, AND CONTROL. Manuscript received April 7, 2009; final manuscript received October 14, 2010; published online April 6, 2011. Assoc. Editor: John R. Wagner.

[3]The "reference signal" in this paper must not be confused with the "reference input" in the control theory context, which generally means a desired output value.

Copyright © 2011 by ASME

Downloaded 06 Apr 2011 to 205.155.65.56. Redistribution subject to ASME license or copyright; see http://www.asme.org/terms/Terms_Use.cfm

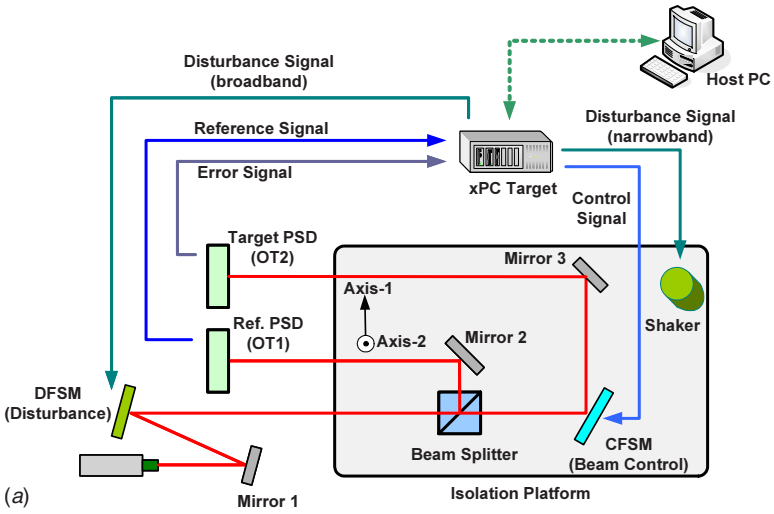

(*a*)

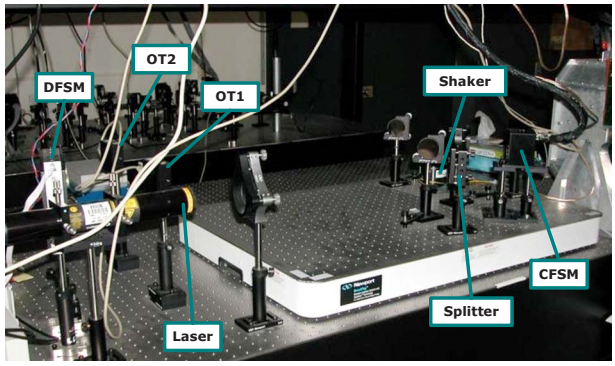

(*b*)

Fig. 1 Laser beam jitter control testbed. (*a*) Schematic; (*b*) photograph.

2 Experimental Setup

Figure 1 shows the optical laser testbed being studied in this project. This testbed is located in the Optical Relay Mirror Lab of the Spacecraft Research and Design Center (SRDC) at Naval Postgraduate School (NPS) in Monterey, CA. The testbed consists of a disturbance injection fast steering mirror (DFSM), a control fast steering mirror (CFSM), two On-Trak position sensing devices (PSDs), namely, OT1 and OT2, one 80/20 beam splitter, three optical folding mirrors, an inertial actuator, and a laser source. Some components are mounted on a Newport vibration isolation platform floated by air pressure. This platform was originally designed to isolate the breadboard from the vibrations of the workbench surface. In our experiment, we use the inertial actuator to vibrate the platform so that the platform simulates a spacecraft or an aircraft equipped with optical systems, which are exposed to mechanical vibrations.

Folding mirror 1 is used to divert the laser beam to the DFSM, which injects the user-defined tip-and-tilt disturbance to the laser beam. The corrupted laser beam then travels through an 80/20 beam splitter, which splits the laser beam into two separate beams. One is sent through the CFSM while the other is reflected on folding mirror 2. Mirror 2 directs the beam to sensor OT1 where the position of the laser beam is measured for the feedforward control. The CFSM is driven by an internal feedback controller, which receives the control commands from an xPC target machine and provides current to the voice coils that tip and tilt the mirror assembly. The CFSM provides the corrective actions to the laser beam as it is reflected by the mirror. The laser beam is then sent to folding mirror 3 and reflected to another sensor OT2, which is the target detector. As shown in Fig. 1(*a*), the horizontal direction is named axis-1, and the vertical direction is named axis-2. More detailed information on these components is available in Refs. [1,9].

It is recognized that using the PSD labeled OT1 is not a normal means to measure the disturbances onboard the platform used to relay the beam as one would not be able to mount a detector separate from the satellite bus in a practical application. However, this reference PSD may be seen as simulating an onboard inertial measurement unit (IMU), which is normally available in satellites with an optical payload. The IMU provides an accurate inertial position of the platform, which is the same as provided by a PSD mounted on a stable reference plane with respect to the vibrating platform. This setup allows an identical measurement without the added cost of an IMU [1].

The control law is designed in the host PC, which is a PC-compatible system with an Intel Pentium processor using MATLAB, version 7.5 release 2007b with SIMULINK and xPC Target Toolbox. The designed control law is compiled and then downloaded to the xPC Target PC, which is another PC-compatible system with an Intel Pentium 4 processor. The Target PC also has PCI-DAS1602/16 (a high-speed 16 bit/16-channel analog input board) and PCIM-DDA06/16 (a high-speed 16 bit/6-channel analog output board), both from Measurement Computing Corporation, Norton, MA, for data acquisition from the PSDs and command output to the FSMs, respectively. A sample rate of 2 kHz was used throughout the experiment, which precluded aliasing of any signals of interest. Increasing the sampling rate more than this value is not beneficial because the control bandwidth of the CFSM driver is limited to about 800 Hz.

Downloaded 06 Apr 2011 to 205.155.65.56. Redistribution subject to ASME license or copyright; see http://www.asme.org/terms/Terms_Use.cfm

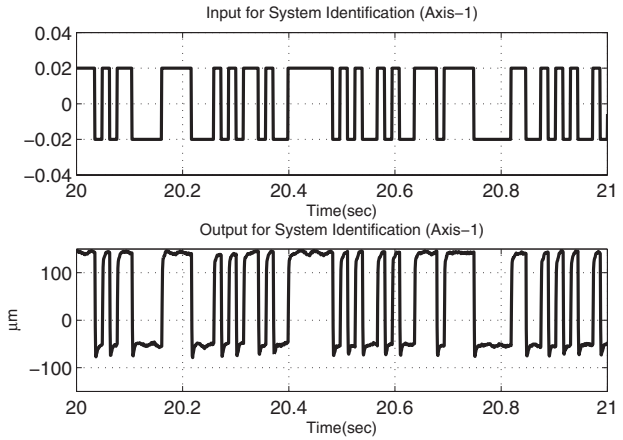

Fig. 2 Input and output signals for system identification (axis-1, magnified)

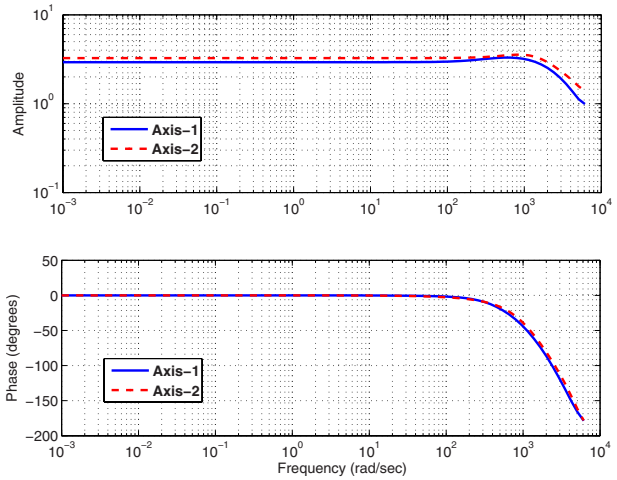

Fig. 3 Bode plot of the identified systems

3 System Identification

As a first step in the design of control methods (for both LTI feedback control and adaptive filter control), we identify an open-loop linear model of the dynamics of the CFSM with its controller. More precisely, we identify an open-loop model from the control input, applied to the CFSM's controller, to the measurement of the beam position at the target while the CFSM internal control loop is closed. Experimental results show that the cross coupling between the two axes of the CFSM and the target position sensor (OT2) is negligible. Therefore, a single-input single-output model of the dynamics of each axis is identified separately to each other.

In the previous work [1,3], the system was assumed to have a predetermined structure and was identified using sinusoidal responses with different frequencies. In this paper, a black-box model is identified by a subspace method using MATLAB and System Identification Toolbox [12]. We chose this method for the following reasons. First, it can directly provide a state-space model, which is required for a LQG controller design. Second, it can result in a discrete-time model, which is better to implement in digital control systems. Lastly, this method does not assume any predetermined structure of the model except for the order of the system, thus giving more flexibility to the identification.

For the input, we use a pseudorandom binary signal (PRBS). The choice of a PRBS has several advantages. For instance, it can excite virtually all the frequency modes [13]. Figure 2 shows the input signal and the resultant output signal trajectory used for the system identification.

From the collected data, System Identification Toolbox provides a third-order, discrete-time state-space model for each axis. The order of the model is selected by trade-off between the performance and the complexity. The CFSM is lightly damped spring-mass system, but most of its flexible modes are attenuated by the CFSM's controller, and the steering mirror (with the internal controller closed) dynamics can be identified as a low order linear model.

The states of this model do not necessarily have any physical meaning. For LQG control with integrator design, we transformed the resultant state-space model to an observable canonical form using a similarity transformation. In this form, the state-space model has one of the state variables as the system's output as follows:

$$\mathbf{x}(k+1) = A\mathbf{x}(k) + Bu(k)$$

$$y(k) = C\mathbf{x}(k) \tag{1}$$

where $\mathbf{x}(k)$, $y(k)$, and $u(k)$ are the state vector, output (position measured at the PSD), and input (applied to the CFSM controller), respectively, at sampling step k and $C=[0 \quad 0 \quad 1]$. The feedthrough matrix D was omitted because there is no direct feedthrough from the control command to the output. Figure 3 shows the frequency response of the identified models.

4 LTI Feedback Control Design

4.1 Linear-Quadratic-Gaussian Control With Integrator. In order to investigate how classical control algorithms handle broadband and narrowband disturbances for the control of laser jitter, a LQG controller is developed. LQG is the combination of a linear quadratic estimator (LQE), or the Kalman filter, with a linear quadratic regulation (LQR). These two can be designed independently. The standard LQR controller is a state regulator, that is, it is designed to drive the states to zero [14]. When there is bias disturbance and/or when the controller needs to force the output to track a nonzero reference, the standard LQG control will have steady-state errors unless the loop gain has at least one integrator. Therefore, we modify the standard LQG design methodology to handle the bias disturbance using integral control as done in Ref. [15] for a continuous-time model. The integral of the error between the output $y(k)$ and the desired output $r(k)$ is generated by the following difference equation:

$$\zeta(k+1) = \zeta(k) + (r(k) - y(k))T_s \tag{2}$$

As done in Refs. [14,15], we can have a difference equation of the states and input errors as follows:

$$\begin{bmatrix} \mathbf{x}_e(k+1) \\ \zeta_e(k+1) \end{bmatrix} = \begin{bmatrix} A & 0 \\ -T_s C & 1 \end{bmatrix} \begin{bmatrix} \mathbf{x}_e(k) \\ \zeta_e(k) \end{bmatrix} + \begin{bmatrix} B \\ 0 \end{bmatrix} u_e(k) \tag{3}$$

where $\mathbf{x}_e(k) = \mathbf{x}(k) - \mathbf{x}_{ss}$, $\zeta_e(k) = \zeta(k) - \zeta_{ss}$, and

$$u_e(k) = u(k) - u_{ss} = -K\mathbf{x}_e(k) + k_I\zeta_e(k) = -K_a \begin{bmatrix} \mathbf{x}_e(k) \\ \zeta_e(k) \end{bmatrix} \tag{4}$$

where $K_a = [K \quad -k_I]$ and the subscript "ss" denotes values at steady-state equilibrium. Since Eqs. (3) and (4) have the standard forms of a state-space difference equation and a linear state feedback control, we can calculate a LQR control gain K_a (and thus K and k_I), which leads to asymptotic stability of the tracking errors. Combining the state feedback control law with a Kalman filter, we can build a LQG feedback control loop.[4] Figure 4 shows a block diagram of the LTI control system.

[4]Note that the standard state-space model with additive white Gaussian system and measurement noises is used in the design, so the designed LQG controller may be suboptimal against the real disturbance in this application.

Downloaded 06 Apr 2011 to 205.155.65.56. Redistribution subject to ASME license or copyright; see http://www.asme.org/terms/Terms_Use.cfm

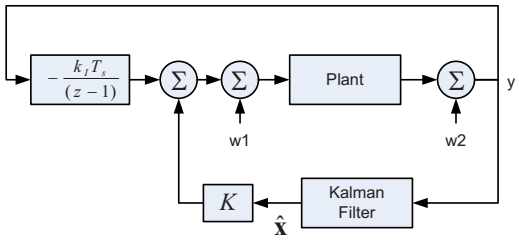

Fig. 4 Block diagram for LQG feedback controller with error integral

4.2 Anti-notch Filter. The performance of the LTI feedback control may be enhanced by means of an anti-notchlike filter when the disturbance has a narrow-bandwidth with a known frequency. Referring to Fig. 5, the output y is related to the setpoint r and disturbance d by

$$y = Tr + Sd \tag{5}$$

where $S=1/(1+PC)$ and $T=PC/(1+PC)$ are the sensitivity and the complementary sensitivity functions, respectively.

Good disturbance rejection requires small gain of the sensitivity function at the disturbance frequency. If we use a filter in series with the controller, it is easy to see that higher filter gain at frequency ω_d will provide higher loop gain at ω_d, which eventually lowers the sensitivity at ω_d. For this purpose, we propose an anti-notchlike filter, or a high-Q bandpass filter, which has high peak gain at the disturbance frequency ω_d, as shown in Fig. 6. Notice that while the standard notch filter, or band-stop filter, attenuates some frequencies to very low levels, the anti-notch filter *amplifies* the frequency of the disturbance. The transfer function of the filter $N(s)$ can be given as

$$N(s) = \frac{s^2 + 2\zeta_1\omega_d s + \omega_d}{s^2 + 2\zeta_2\omega_d s + \omega_d} \tag{6}$$

where $\zeta_1 > \zeta_2$.

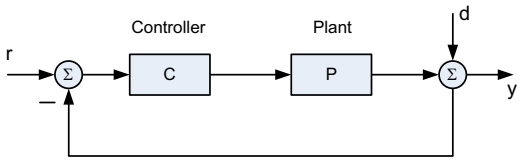

Fig. 5 Block diagram for simple feedback control loop

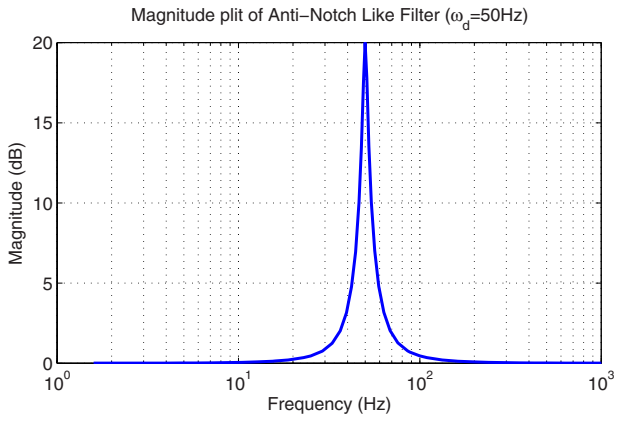

Fig. 6 Magnitude plot of anti-notchlike filter (ω_d=50 Hz)

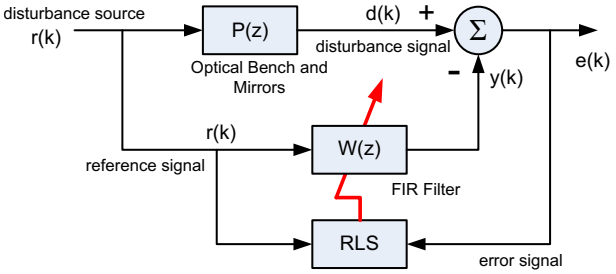

Fig. 7 Block diagram for simplified RLS implementation

5 Adaptive Filter Design

The LTI controller designed in the previous section is a feedback-type control method, which uses only feedback of the output error to calculate the control input. We can significantly improve jitter control performance by employing feedforward-type control methods when reference signals, which are highly correlated with disturbance, are available.

5.1 Recursive-Least-Squares Algorithm. Instead of the LMS algorithm that was used in the previous work [1], the RLS algorithm can be used with a transversal filter to provide faster convergence and smaller steady-state error [10]. The rate of convergence of the RLS algorithm is typically an order of magnitude faster than that of the LMS algorithm [11]. The RLS algorithm generally requires more computational burden than the LMS algorithm, but the current development of computer hardware enables us to use it in real-time application. In addition, it is well known that the RLS algorithm is less robust than the LMS algorithm. See Refs. [10,11] for more detailed comparison between RLS and LMS algorithms.

A reference signal, correlated with disturbance, is input to a transversal filter consisting of M taps. The error between the desired beam location at the target and the actual location is fed back to the filter to adjust these taps. The reference signal is generated by the output of the feedforward PSD (OT1), and the error is generated by the output of the target PSD (OT2), both are sampled at a rate of 2 kHz. The output of the transversal filter is used as a control signal to the CFSM. Figure 7 shows the simplified standard RLS implementation for disturbance rejection.

The reference signal $r(n)$ is delayed one time step for each of the $M-1$ delays, excluding the current input, forming a vector of delayed inputs, $\mathbf{r}(n) \triangleq [r(n), r(n-1), \ldots, r(n-M+1)]^T \in \mathbb{R}^M$. The inner product of the vector of tap gains, $\mathbf{w}(n) = [w_0(n), \ldots, w_{M-1}(n)]^T \in \mathbb{R}^M$, and the vector of delayed inputs, $\mathbf{r}(n)$, produces the scalar filtered output $y(n)$:

$$y(n) = \sum_{i=0}^{M-1} w_i(n-1)r(n-i) = \mathbf{w}^T(n-1)\mathbf{r}(n) \tag{7}$$

The error signal at time instant n is determined by

$$e(n) \triangleq d(n) - y(n) \tag{8}$$

The RLS algorithm to update the weighting vector, $\mathbf{w}(n)$, at each instance is given as follows [11,16]:

$$\mathbf{k}(n) = \frac{\lambda^{-1}\mathbf{P}(n-1)\mathbf{r}(n)}{1 + \lambda^{-1}\mathbf{r}^T(n)\mathbf{P}(n-1)\mathbf{r}(n)} \tag{9}$$

$$\mathbf{w}(n) = \mathbf{w}(n-1) + \mathbf{k}^T(n)e(n) \tag{10}$$

$$\mathbf{P}(n) = \lambda^{-1}\mathbf{P}(n-1) - \lambda^{-1}\mathbf{k}(n)\mathbf{r}^T(n)\mathbf{P}(n-1) \tag{11}$$

where $\mathbf{k}(n) \in \mathbb{R}^M$ is the time-varying gain vector and $\mathbf{P}(n) \in \mathbb{R}^{M\times M}$ is the inverse correlation matrix, which is an inverse of the weighted autocorrelation matrix for $x(n)$.

Downloaded 06 Apr 2011 to 205.155.65.56. Redistribution subject to ASME license or copyright; see http://www.asme.org/terms/Terms_Use.cfm

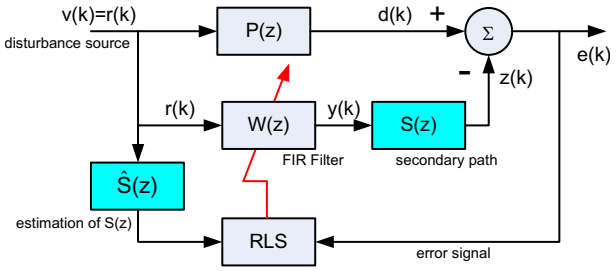

Fig. 8 Block diagram for FXRLS implementation

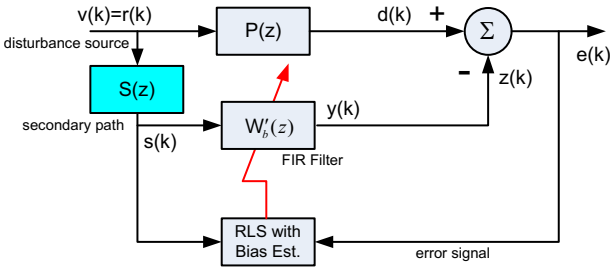

Fig. 9 Equivalent diagram of FXRLS implementation when $\hat{S}(z)=S(z)$

5.2 Filtered-X RLS Algorithm. The RLS algorithm described in the previous section assumes that the error signal is the difference between the disturbance signal and the output of the adaptive filter, as shown in Fig. 7. However, in real jitter control systems, there is a secondary path through which the output of the RLS filter must go. For instance, the output of the filter is applied to the CFSM to correct the beam in the testbed. This secondary path must be modeled in the control algorithm to take into account the delays and other effects that occur to the control signal. Without this consideration, the RLS algorithm may not properly control the beam. We observed that the weighting vector, $\mathbf{w}(n)$, becomes unstable when the standard RLS algorithm is used in the testbed.

In order to properly make use of the RLS algorithm, a copy of the secondary plant transfer function is placed in the path to the updating algorithm for the weight vector. This method is referred to as the FXRLS algorithm [10]. Figure 8 shows a block diagram of the jitter control system using the FXRLS algorithm.

5.3 Integrated Bias Estimation With FXRLS Algorithm. In practical cases, the disturbance signal may contain a dc component or constant bias disturbance. The reference signal may also have a dc component. Let us assume that the reference signal $r(n)$ at a quasi-steady-state consists of a dc component r_0 and a zero-mean broadband/narrowband noise term $\hat{r}(n)$, that is,

$$r(n) = r_0 + \hat{r}(n) \tag{12}$$

Then, the Finite Impulse Response (FIR) filter output can be written as

$$y(n) = r_0 \sum_{i=0}^{M-1} w_i(n-1) + \mathbf{w}^T(n-1)\hat{\mathbf{r}}(n) \tag{13}$$

where $\hat{\mathbf{r}}(n)=[\hat{r}(n),\ldots,\hat{r}(n-M+1)]^T$. If the updated weighting vector $\mathbf{w}(n)$ reaches a quasi-steady state, we can say that $w_i(n)=w_i$ for $i=0,\ldots,M-1$. Then, if we calculate a dc component of $y(n)$ by taking its average, we have a constraint on the filter gains for complete disturbance cancellation as

$$\bar{y} = r_0 \sum_{i=0}^{M-1} w_i = \bar{d} \tag{14}$$

where $\bar{d}$ is a dc component of the disturbance. If the reference signal's dc component, r_0, is very small, the sum of filter coefficients w_i must be very large. Even in worse case, if $r_0=0$, then the adaptive filter will be unable to completely cancel the bias disturbance.

In most laser targeting schemes, an additional compensator is used to correct the bias error at the target. For instance, in previous work [1], an additional adaptive filter, called the ABF, was used to calculate a proper bias term. Then, it was added to the reference signal. Gibson, Tsao, and their colleague [2,4–6] used additional LTI control loop to erase the biased disturbance term. These methods require extra control blocks and thus increase complexity of control systems. In this paper, we propose a simple method, which has an integrated bias estimator to handle the bias disturbance. This method does not need any additional filter or control block.

We obtain the bias estimation conveniently by augmenting a nonzero constant (e.g., 1) to the reference signal vector $\mathbf{r}(n)$ and by also augmenting a weight coefficient corresponding to this augmented reference element. More concretely, we can define a new reference signal vector and a weight vector as

$$\mathbf{r}_b(n) \triangleq [1,\mathbf{r}^T(n)]^T = [1,r(n),r(n-1),\ldots,r(n-M+1)]^T \tag{15}$$

$$\mathbf{w}_b(n) \triangleq [w_b(n),\mathbf{w}^T(n)]^T = [w_b(n),w_0(n),w_1(n),\ldots,w_{M-1}(n)]^T, \tag{16}$$

apply the adaptive algorithm to update the new weight vector $\mathbf{w}_b(n)$, and obtain a dc component w_b at the output of the filter.

As in the previous section, the filter output needs to pass a secondary path to correct beam jitter, and thus we need to take this effect into account. Figure 9 shows a virtual equivalent diagram of the FXRLS algorithm when the identified model of the secondary path, $\hat{S}(z)$, is close enough to the actual path, $S(z)$, i.e., $\hat{S}(z)=S(z)$ [10]. In this figure, the RLS algorithm will calculate the weight vector $\mathbf{w}_b'(n)$, which reduces the tracking error $e(z)$ using the filter output $y(n)=\mathbf{w}_b'^T(n-1)\mathbf{s}_b(n)$, where $\mathbf{s}_b(n)=[1,\mathbf{s}^T(n)]^T$. The dc component of $y(n)$ is then

$$\bar{y} = \bar{s}\sum_{i=0}^{M-1} w_i' + w_b' = S(1)\bar{v}\sum_{i=0}^{M-1} w_i' + w_b' \tag{17}$$

where $S(1)$ is a dc gain of $S(z)$. On the other hand, in the actual FXRLS system shown in Fig. 8, the dc component of the output of the filter is

$$\bar{y} = \bar{v}\sum_{i=0}^{M-1} w_i + w_b \tag{18}$$

After passing through the secondary path $S(z)$, the dc component of the correction effort $z(n)$ becomes

$$\bar{z} = S(1)\bar{v}\sum_{i=0}^{M-1} w_i + S(1)w_b \tag{19}$$

Comparing Eqs. (17) and (19), we can see that $w_i(n)=w_i'(n)$ as in the conventional FXRLS algorithm without the bias weight, but the weight coefficient for bias, $w_b(z)$, needs to be scaled as

$$w_b(n) = \frac{w_b'(n)}{S(1)} \tag{20}$$

Downloaded 06 Apr 2011 to 205.155.65.56. Redistribution subject to ASME license or copyright; see http://www.asme.org/terms/Terms_Use.cfm

Table 1 Disturbance characteristics

Bias (dc)	Narrowband	Broadband
~1000 μm	50 Hz mechanical vibration	200 Hz band-limited white noise (DFSM)

6 Experimental Results

Several experiments with various scenarios were ran on the testbed at NPS to explore the capabilities of the proposed control methods. The control and filtering sampling rate was 2 kHz, and the forgetting factor for all FXRLS filters was $\lambda = 0.99999$. Table 1 summarizes the characteristics of the disturbances used in the experiments. These disturbance components are injected separately or together, depending on the scenarios.

6.1 Effect of Integrated Bias Estimator. In order to see the integrated bias estimator effect, three control methods are compared: The first is a 20th-order FXRLS filter without the BE, the second is a parallel combination of the FXRLS filter and LQG controller (to correct the bias error), and the third is a 20th-order FXRLS filter with the integrated BE. (In the design of the second controller, the interaction between two control loops is not considered.) The reference signal measured at OT1 is unbiased by subtracting a dc component and then fed into the adaptive filter. The DFSM is used to inject a mixture of a bias disturbance and a broadband random noise of 200 Hz band-limited white noise to simulate the effect of atmospheric turbulence.

Figure 10 shows the time series of beam position measured at the target PSD (OT2) with different control methods. The controllers are activated at $t = 5$ s. The FXRLS filter without BE cannot correct the bias disturbance using the unbiased reference signal, as expected in Sec. 5.3, and the system becomes unstable. By combining the FXRLS filter with the LQG, the bias disturbance is corrected, but the controller cannot correct the broadband noise well. The FXRLS filter with BE can control the bias component as well as the broadband random components. From this experiment, we can conclude that the FXRLS filter with BE is simpler and has better performance than the combination of FXRLS (without BE) and LQG for both broadband and bias disturbances. The part of reason is that the FXRLS and LQG loops are designed separately and connected in parallel without considering the interaction between these two loops.

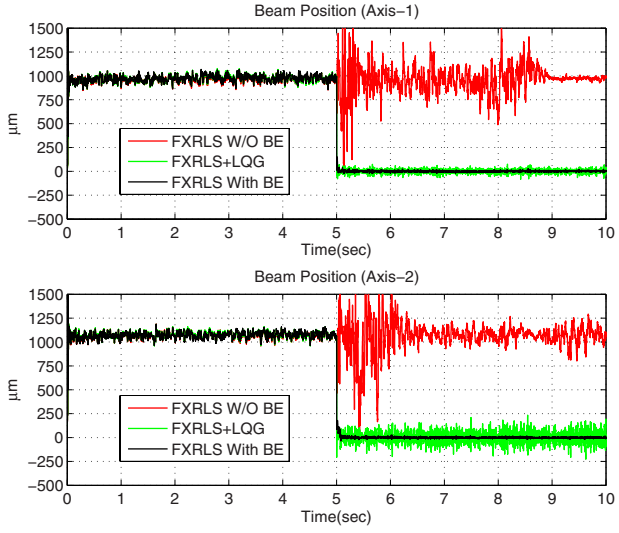

Fig. 10 Comparison of beam position errors

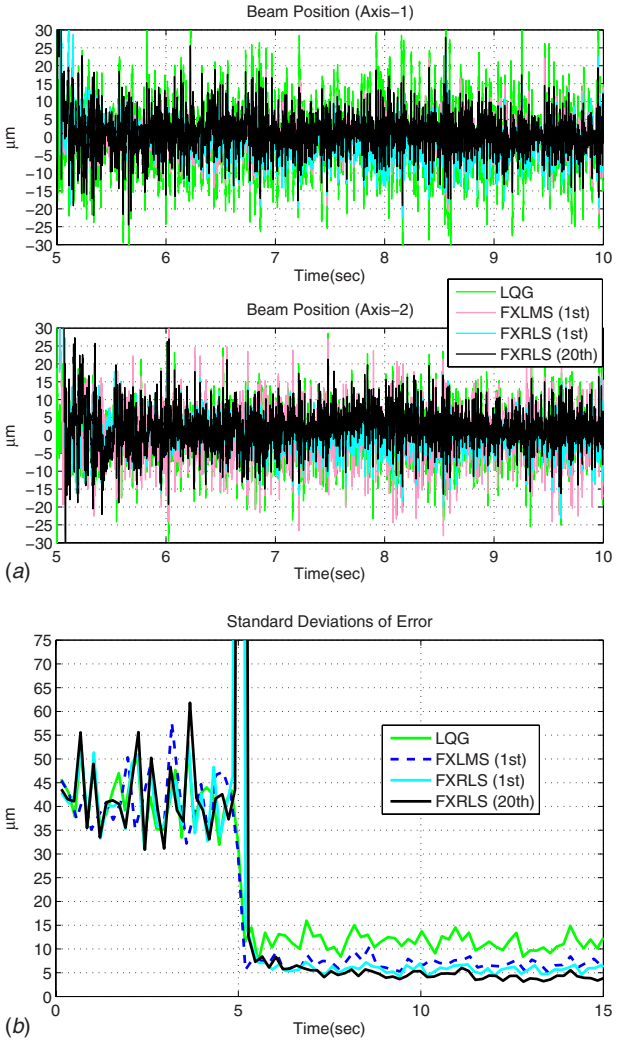

Fig. 11 Comparison of controllers for broadband noises

6.2 Broadband Random Noise Disturbance. In this experiment, LQG (with integral control), FXLMS filter (without BE), and FXRLS filters (with BE) are compared with 200 Hz band-limited white noise. The reference signal, however, is not unbiased so that the FXLMS filter can be operational without the bias estimator. After running experiments with different numbers of orders, the first-order filter was found to be optimum for the FXLMS controller. The experimental results are shown in Fig. 11, where the standard deviation is calculated from each set of 50 sampled data points. Both adaptive filters show better performance than LQG feedback control. While performance of the FXLMS algorithm becomes slightly degraded as the filter order increases, performance of the FXRLS algorithm becomes slightly improved. Even with the smallest number of the taps (i.e., one tap with the bias estimator), the FXRLS algorithm shows superior performance over the FXLMS. Table 2 provides a quantitative comparison of the various control methods for the broadband random noises.

6.3 Narrowband Vibrational Disturbance. While the broadband noise is caused by the atmospheric turbulence, narrowband jitter is generally created by mechanical vibrations. In this experiment, an inertial actuator vibrates the floating platform at 50 Hz (=3000 rpm) frequency. This frequency is in the range of the typical spinning speed of flywheel actuators used for spacecraft attitude control. The LQG controller with anti-notch filter is also compared along with the LQG, FXLMS, and FXRLS control

Downloaded 06 Apr 2011 to 205.155.65.56. Redistribution subject to ASME license or copyright; see http://www.asme.org/terms/Terms_Use.cfm

Table 2 Comparison of control methods for broadband noises

Controller		LQG	FXLMS (1st)	FXRLS (1st)	FXRLS (20th)
Input jitter	Axis-1	31.70	31.93	31.93	31.92
(standard deviation, μm)	Axis-2	32.50	32.44	32.20	32.37
Controlled error	Axis-1	9.07	4.44	4.47	3.09
(standard deviation, μm)	Axis-2	7.15	5.32	4.18	2.92

Table 3 Comparison of control methods for narrowband disturbance

Controller		LQG	LQG+ anti-notch	FXLMS (1st)	FXRLS (20th)
Input jitter	Axis-1	21.32	20.36	20.46	20.56
(standard deviation, μm)	Axis-2	38.70	38.33	38.33	38.36
Controlled error	Axis-1	8.66	4.58	9.52	3.54
(standard deviation, μm)	Axis-2	12.68	2.82	13.20	2.28

methods. The anti-notch filter is designed with assumption that the mechanical vibrational frequency is known. Since the anti-notch filter is simply cascaded with the existing LQG controller, the combined controller is not optimal anymore and its stability is not guaranteed. However, as shown in Fig. 12(*a*), the anti-notch filter effectively attenuates the narrowband frequency disturbance at 50 Hz, compared with the LQG-alone controller. As shown in Figs. 12(*b*) and 12(*c*), the FXRLS filter attenuates the narrowband disturbance more than the LQG plus the anti-notch filter controller, even though the FXRLS filter does not need to know the vibrational frequency. (The spike at 120 Hz in Fig. 12(*b*) could be harmonic.) Table 3 provides a quantitative comparison of the various control methods for the narrowband disturbance.

6.4 Broadband and Narrowband Disturbance. Finally, for the most general case, both the mechanical vibration disturbance by the shaker and broadband/bias disturbance by DFSM are injected to the system. In this experiment, the FXRLS filter shows slightly better performance than the LQG plus anti-notch filter controller, even though it does not need any information on the vibrational frequency. See Fig. 13 and Table 4 for the experimental result data.

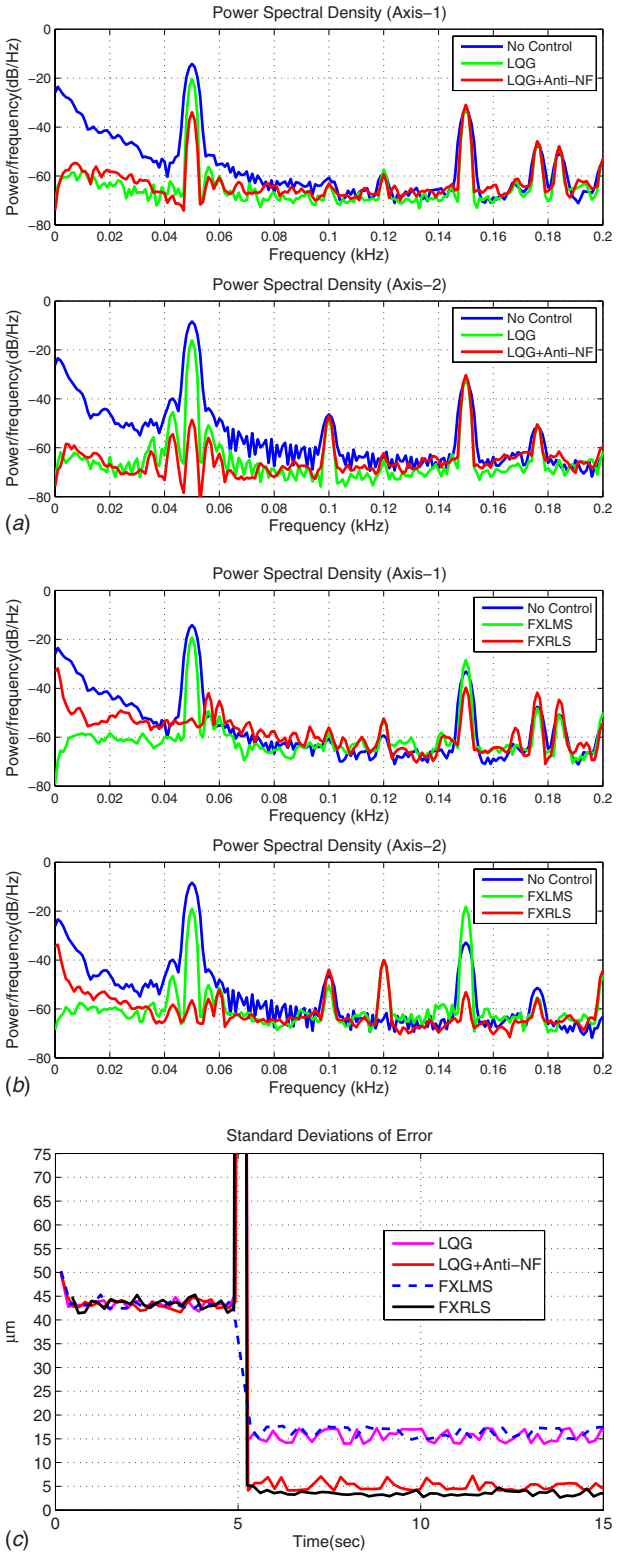

Fig. 12 Comparison of controllers for narrowband disturbance

7 Conclusions

The jitter attenuation problem for an optical laser testbed located at the Naval Postgraduate School was considered and the possibility of using feedforward adaptive filter techniques was investigated. We proposed a FXRLS adaptive filter, which contains an integrated bias estimator. This configuration simplifies the controller's complexity by removing an additional control block for bias correction. The developed method has been compared with other conventional LTI controller and FXLMS adaptive filters through experimental results. The FXRLS adaptive filter showed superior performance both in narrowband and broadband disturbance jitter controls. The integrated bias estimator is effective especially when the reference signal has a very small dc component.

The developed algorithm has a simpler structure than the lattice filter, but shows good jitter rejection performance. It needs, however, a reference signal, which contains real-time information regarding the disturbance. For some practical applications in which such a reference signal is not available, it would be beneficial to develop adaptive methods, which use the target error signal only, and this is suggested for future research.

Downloaded 06 Apr 2011 to 205.155.65.56. Redistribution subject to ASME license or copyright; see http://www.asme.org/terms/Terms_Use.cfm

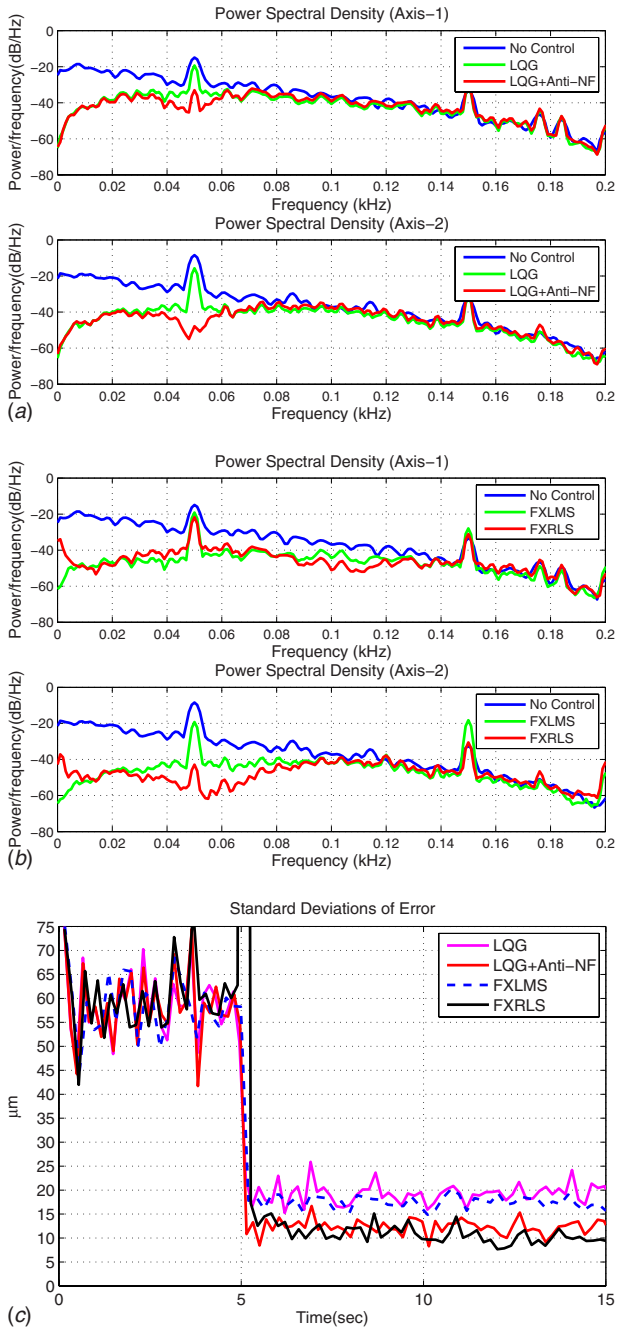

Fig. 13 Comparison of controllers for broadband/narrowband disturbance

Table 4 Comparison of control methods for broadband/narrowband disturbance

Controller		LQG	LQG+ anti-notch	FXLMS (1st)	FXRLS (20th)
Input jitter	Axis-1	35.71	36.34	36.29	35.87
(standard deviation, μm)	Axis-2	49.69	49.52	49.81	49.62
Controlled error	Axis-1	12.91	9.58	10.52	8.84
(standard deviation, μm)	Axis-2	14.82	7.62	13.91	5.42

References

[1] Watkins, R. J., and Agrawal, B. N., 2007, "Use of Least Means Squares Filter in Control of Optical Beam Jitter," J. Guid. Control Dyn., **30**(4), pp. 1116–1122.

[2] Orzechowski, P. K., Gibson, J. S., and Tsao, T.-C., 2004, "Optimal Disturbance Rejection by LTI Feedback Control in a Laser Beam Steering System," Proceedings of the 43rd IEEE Conference on Decision and Control, Atlantis, Paradise Island, Bahamas, pp. 2143–2148.

[3] Bateman, B. E., 2007, "Experiments on Laser Beam Jitter Control With Applications to a Shipboard Free Electron Laser," MS thesis, Naval Postgraduate School, Monterey, CA.

[4] Pérez Arancibia, N. O., Chen, N. Y., Gibson, J. S., and Tsao, T.-C., 2006, "Variable-Order Adaptive Control of a Microelectromechanical Steering Mirror for Suppression of Laser Beam Jitter," Opt. Eng. (Bellingham), **45**(10), p. 104206.

[5] Orzechowski, P. K., Chen, N., Gibson, S., and Tsao, T.-C., 2006, "Optimal Jitter Rejection in Laser Beam Steering With Variable-Order Adaptive Control," Proceedings of the 45th IEEE Conference on Decision and Control, San Diego, CA, pp. 2057–2062.

[6] Pérez Arancibia, N. O., Chen, N., Gibson, S., and Tsao, T.-C., 2006, "Adaptive Control of Jitter in Laser Beam Pointing and Tracking," Proc. SPIE, **6304**, p. 63041G.

[7] Jiang, S.-B., and Gibson, S., 1995, "An Unwindowed Multichannel Lattice Filter With Orthogonal Channels," IEEE Trans. Signal Process., **43**(12), pp. 2831–2842.

[8] McEver, M. A., Cole, D. G., and Clark, R. L., 2004, "Adaptive Feedback Control of Optical Jitter Using q-Parameterization," Opt. Eng. (Bellingham), **43**(4), pp. 904–910.

[9] Watkins, R. J., 2004, "The Adaptive Control of Optical Beam Jitter," Ph.D. thesis, U.S. Naval Postgraduate School, Monterey, CA.

[10] Kuo, S. M., and Morgan, D. R., 1996, *Active Noise Control Systems: Algorithms and DSP Implementations*, Wiley-Interscience, New York.

[11] Haykin, S., 2001, *Adaptive Filter Theory*, 4th ed., Prentice-Hall, Upper Saddle River, NJ.

[12] Ljung, L., 2007, *System Identification Toolbox 7, User's Guide*, The MathWorks, Inc., Natick, MA.

[13] Ljung, L., 1999, *System Identification—Theory for the User*, 2nd ed., Prentice-Hall, Upper Saddle River, NJ.

[14] Burl, J. B., 1998, *Linear Optimal Control,* H_2 *and* H_∞ *Methods*, 1st ed., Prentice-Hall, Upper Saddle River, NJ.

[15] Ogata, K., 1996, *Modern Control Engineering*, 3rd ed., Prentice-Hall, Upper Saddle River, NJ.

[16] 2007, *Signal Processing Blockset 6, User's Guide*, The MathWorks Inc., Natick, MA.

Downloaded 06 Apr 2011 to 205.155.65.56. Redistribution subject to ASME license or copyright; see http://www.asme.org/terms/Terms_Use.cfm